Experimental investigation of pulse generation with one-pump fiber optical parametric amplification

Armand A. Vedadi,* Mohammad Amin Shoaie, and Camille-Sophie Brès

Photonic Systems Laboratory (PHOSL), STI-IEL, Ecole Polytechnique Fédérale de Lausanne (EPFL), CH-1015 Lausanne, Switzerland

*armand.vedadi@epfl.ch

Abstract: In a recent study, the theory of pulse generation with fiber optical parametric amplification using sinusoidal (clock) intensity modulated pump was revisited [J. Lightwave Technol. **30**, 1263 (2012)] [1]. This work showed that the pulses generated through such parametric interaction exhibit a shape which depends on the signal detuning with respect to the pump position (i.e. linear phase mismatch). A near Gaussian shape can only be achieved over a small region of the gain spectrum, close to the maximum gain location. Towards the extremities of the gain spectrum, the generated pulses take a near Sinc shape which can have many potential applications such as for all-optical Nyquist limited transmitters and/or receivers. In this paper we experimentally verify the theory at repetition rates up to 40 GHz. We also discuss the impact of noise, pump saturation and walk-off on the generated pulses.

OCIS codes: (060.4370) Nonlinear optics, fibers; (060.2320) Fiber optics amplifiers and oscillators.

References and links

1. A. Vedadi, A. Ariaei, M. M. Jadidi, and J. A. Salehi, "Theoretical study of high repetition rate short pulse generation with fiber optical parametric amplification," J. Lightwave Technol. **30**, 1263–1268 (2012).
2. H. Hu, H. C. H. Mulvad, C. Peucheret, M. Galili, A. Clausen, P. Jeppesen, , and L. K. Oxenlowe, "10 GHz pulse source for 640 Gbit/s OTDM based on phase modulator and self-phase modulation," Opt. Express **19**, 343–349 (2011).
3. J. Li, J. Hansryd, P. Hedekvist, P. Andrekson, and S. Knudsen, "300-Gb/s eye-diagram measurement by optical sampling using fiber-based parametric amplification," IEEE Photon. Technol. Lett. **13**, 987–989 (2001).
4. A. Otani, Y. Tsuda, K. Igawa, and K. Shida, "Novel optical sampling oscilloscope using envelope detection triggering method," J. Lightwave Technol. **26**, 2991–2998 (2008).
5. M. Jamshidifar, A. Vedadi, D. S. Govan, and M. E. Marhic, "Continuous-wave parametric amplification in bismuth-oxide fibers," Opt. Fiber Technol. **16**, 458–466 (2010).
6. B.-P. Kuo, A. Wiberg, C.-S. Brés, N. Alic, and S. Radic, "Ultrafast clock recovery and sampling by single parametric device," IEEE Photon. Technol. Lett. **23**, 191–193 (2011).
7. J. Hansryd and P. Andrekson, "Wavelength tunable 40GHz pulse source based on fibre optical parametric amplifier," IEE Electron. Lett. **37**, 584–585 (2001).
8. T. Torounidis, M. Karlsson, and P. A. Andrekson, "Fiber optical parametric amplifier pulse source: Theory and experiments," J. Lightwave Technol. **23**, 4067–4073 (2005).
9. T. Torounidis, M. Westlund, H. Sunnerud, B.-E. Olsson, and P. Andrekson, "Signal generation and transmission at 40, 80, and 160 Gb/s using a fiber-optical parametric pulse source," IEEE Photon. Technol. Lett. **17**, 312–314 (2005).

#174838 - $15.00 USD Received 23 Aug 2012; revised 15 Oct 2012; accepted 5 Nov 2012; published 19 Nov 2012

10. G.-W. Lu, K. Abedin, T. Miyazaki, and M. Marhic, "RZ-DPSK OTDM demultiplexing using fibre optical parametric amplifier with clock-modulated pump," IEE Electron. Lett. **45**, 221–222 (2009).
11. A. A. Vedadi and C.-S. Bres, "Experimental investigation of fiber optical parametric amplifier pulse generators," in "Nonlinear Photonics," (Optical Society of America, 2012), p. JM5A.8.
12. A. S. Y. Hsieh, G. K. L. Wong, S. G. Murdoch, S. Coen, F. Vanholsbeeck, R. Leonhardt, and J. D. Harvey, "Combined effect of Raman and parametric gain on single-pump parametric amplifiers," Opt. Express **15**, 8104–8114 (2007).
13. E. Lichtman, A. A. Friesem, R. G. Waarts, and H. H. Yaffe, "Exact solution of four-wave mixing of copropagating light beams in a kerr medium," J. Opt. Soc. Am. B **4**, 1801–1805 (1987).
14. Marhic, *Fiber Optical Parametric Amplifiers, Oscillators and Related Devices* (Cambridge, 2007).
15. D. Dahan and G. Eisenstein, "Tunable all optical delay via slow and fast light propagation in a Raman assisted fiber optical parametric amplifier: a route to all optical buffering," Opt. Express **13**, 6234–6249 (2005).
16. N. Nasser, G. Fanjoux, E. Lantz, and T. Sylvestre, "Tunable optical delay using parametric amplification in highly birefringent optical fibers," J. Opt. Soc. Am. B **28**, 2352–2357 (2011).
17. A. Mussot, A. Kudlinski, E. Louvergneaux, M. Kolobov, and M. Taki, "Impact of the third-order dispersion on the modulation instability gain of pulsed signals," Opt. Lett. **35**, 1194–1196 (2010).
18. A. Vedadi, M. A. Shoaie, and C.-S. Brés, "Near nyquist sinc optical pulse generation with fiber optical parametric ampification," in "European Conf. on Optical Comm. 2012," (2012), P1.10.
19. A. Durécu-Legrand, C. Simonneau, D. Bayart, A. Mussot, T. Sylvestre, E. Lantz, and H. Maillotte, "Impact of pump OSNR on noise figure for fiber-optical parametric amplifiers," IEEE Photon. Technol. Lett. **17**, 1178–1180 (2005).
20. A. Mussot, A. Durécu-Legrand, E. Lantz, C. Simmoneau, D. Bayart, H. Maillotte, and T. Sylvestre, "Impact of pump phase modulation on the gain of fiber parametric amplifier," IEEE Photon. Technol. Lett. **16**, 1289–1291 (2004).

1. Introduction

Over the last decades, we have witnessed a substantial growth in streaming video/audio, high definition television and many more bandwidth hungry applications with no apparent slowing down. With the ever increasing demand for bandwidth in today's constantly growing network, extensive research efforts have been focused on advanced modulation formats capable of carrying more bits of information per symbol. In addition, it is also expected that transmission capacity will be increased by making wideband wavelength division multiplexed (WDM) systems and increasing the data bitrate per wavelength channel. In comparison with broader dense WDM systems, the former enables a simplified network control due to fewer channels. Undeniably, high repetition rate ultrashort pulse generators are a key enabling device for the future high capacity flexible optical networks [2]. Mode-locked fiber lasers (MLL) represent a potential source of such pulses and to date, the vast majority of optical pulse sources related applications have been based on MLL [3–6]. However stringent phase locking condition renders their operation non-trivial and prone to external perturbations. As a result, mode-locked sources require complex and rigorous phase locking arrangements to maintain stability. Moreover, pulse repetition rate is usually limited by the bandwidth of the intra-cavity modulator while the limited bandwidth of the gain medium constrains wavelength tunability. Another technique is to use a fiber optic parametric amplifier (FOPA) driven by a sinusoidally intensity modulated pump coupled with a continuous wave (CW) signal [7,8]. A pulsed idler with identical repetition rate as the pump but compressed characteristics is generated through four wave mixing (FWM). Demonstrations of such source with important applications to high bit rate RZ signal generation and optical time division multiplexing/demultiplexing have been reported [9, 10].

In a recent theoretical investigation [1], it was found that the generated pulse shape depends on the linear phase matching $\Delta\beta_L$ between the pump, signal and idler waves. In particular, it was theoretically proven that the shortest pulses are generated when $\Delta\beta_L = -4\gamma P_0$, where γ is the fiber nonlinear coefficient and P_0 is the pump peak power inside the fiber. When such condition is satisfied, the generated pulse on the idler side exhibits a Sinc-like function shape with a full width half maximum (FWHM) inversely proportional to $\gamma P_0 L$, L the length of the

#174838 - $15.00 USD Received 23 Aug 2012; revised 15 Oct 2012; accepted 5 Nov 2012; published 19 Nov 2012

fiber. The generally assumed Gaussian shape is only valid in the case of perfect phase matching (i.e. $\Delta\beta_L = -2\gamma P_0$). In that case the FWHM is inversely proportional to $\sqrt{\gamma P_0 L}$. In [11] we have shown the first experimental verification of these theoretical results. The pulse width and shape for increasing pump powers in the two aforementioned phase matching cases at 2.5 GHz repetition rate were measured showing an excellent agreement between theory and practice. In this article, we extend the previous work and perform near-Sinc shape pulse generation at up to 40 GHz repetition rate, in excellent agreement with both theory and simulations. In additon, we look at the impact of walk off on the quality of pulse generation in FOPAs.

2. Theory

In this section, the equations of [1] are driven using a more rigorous formulation with the aim of delimiting the domain of validity of these equations. We consider a pump, signal and idler waves co-propagating in a highly nonlinear fiber (HNLF) at angular frequencies ω_P, ω_S and ω_I, respectively. In the most general case, we allow the pump, signal and idler slowly varying envelopes (SVE) $A_P(z,\tau)$, $A_S(z,\tau)$ and $A_I(z,\tau)$ to evolve in time. Neglecting absorption and Raman scattering, the propagation of the waves inside the HNLF can be modeled by the nonlinear Schrödinger equation:

$$\frac{\partial A}{\partial z} = j\{\sum_{k=2}^{\infty} \frac{\beta_k}{k!} \frac{\partial^k A}{\partial \tau^k} + \gamma |A|^2 A\} \tag{1}$$

Equation (1) is written in a frame moving at the pump group velocity ($\tau = t - z\beta_1$). γ is the fiber nonlinearity coefficient and β_k is the k^{th} derivative of the propagation constant at ω_P. For a standard HNLF, knowledge of the dispersion β_2, dispersion slope β_3 and dispersion curvature β_4 is sufficient to describe the physical processes with good accuracy. A is the SVE of the total electical field propagating in the fiber: $A(z,\tau) = A_P(z,\tau) + A_S(z,\tau)e^{j\Delta\omega_S\tau} + A_I(z,\tau)e^{-j\Delta\omega_S\tau}$ with $\Delta\omega_S = \omega_I - \omega_P = \omega_P - \omega_S$. Note that here we allow $\Delta\omega_S$ to be negative. Also, in neglecting Raman, we have assumed that $\Delta\omega_S$ remains small compared to the Raman shift. This is no longer true for high fiber nonlinearity or FOPA pump power, in which case it is necessary to take into account the Raman contribution [12]. We assume that the pump remains undepleted ($|A_P| >> |A_S|$) and we rearrange the terms at pump, signal and idler frequencies:

$$\begin{aligned}
\frac{\partial A_P}{\partial z} &= j\{\textstyle\sum_{k=2}^{4} \frac{\beta_k}{k!} \frac{\partial^k A_P}{\partial \tau^k} + \gamma |A_P|^2 A_P\} \\
\frac{\partial A_S}{\partial z} &= j\{\textstyle\sum_{k=2}^{4} \frac{\beta_k}{k!} \left[\sum_{m=0}^{k} C_k^m \frac{\partial^m A_S}{\partial \tau^m} \left(j\Delta\omega_S\right)^{k-m}\right] + \gamma A_P^2 A_I^*\} \\
\frac{\partial A_I}{\partial z} &= j\{\textstyle\sum_{k=2}^{4} \frac{\beta_k}{k!} \left[\sum_{m=0}^{k} C_k^m \frac{\partial^m A_I}{\partial \tau^m} \left(-j\Delta\omega_S\right)^{k-m}\right] + \gamma A_P^2 A_S^*\},
\end{aligned} \tag{2}$$

where C_k^m are the binomial coefficients defined as $\frac{k!}{m!(k-m)!}$. This system of equations (2) is valid as long as the pump is not depleted. The first terms on the right of each of these equations account for dispersion related phenomona. They depend on the shape of the SVE through its time derivatives. We now consider that the pump is intensity modulated by a single RF tone at repetition rate f_R. Using either an electro-absorption modulator or an Mach-Zehnder modulator operated at the quadrature bias point, the pump power at the fiber input writes as $P_P(0,\tau) = P_0 \times 1/2\,(1 + cos(2\pi f_R t)) = P_0 cos^2(\pi f_R t)$. The pump amplitude can then be written as $A_P = \sqrt{P_0} cos(\pi f_R t)$, where the pump initial phase was arbitrary set to zero without loss of generality.

When the dispersion length $L_D = 1/\sum_{k=2}^{4} \frac{\beta_k}{k!} (2\pi f_R)^k$ is long compared to the nonlinear length $L_{NL} = 1/(\gamma P_0)$, only the self-phase modulation term in the first equation of Eq. (2) can be considered [13]. The output pump field then writes as:

$$A_P(L,\tau) = \sqrt{P_0} \cos(\pi f_R \tau) e^{j\gamma P_0 \cos^2(\pi f_R \tau) L} \tag{3}$$

#174838 - $15.00 USD Received 23 Aug 2012; revised 15 Oct 2012; accepted 5 Nov 2012; published 19 Nov 2012

In order to solve the equations for signal and idler in Eq. (2), we assume that the bandwidth of both signal and idler waves remain negligible compared to $\Delta\omega_S$ throughout the HNLF. In this case, the signal and idler SVE time derivatives can be neglected and the system of equations become similar to the standard FOPA equations for signal and idler [14]. The HNLF idler output SVE can then be derived as:

$$A_I(L,\tau) = jA_S^*(0)\frac{\gamma P_0 \cos^2(\pi f_R \tau)}{g}\sinh(gL) \times e^{j\left\{\gamma P_0 \cos^2(\pi f_R \tau)+\frac{\beta_3}{6}\Delta\omega_S{}^3\right\}L} \tag{4}$$

where $g^2 = (\gamma P_0 \cos^2(\pi f_R \tau))^2 - (\kappa/2)^2$. $\kappa = 2\gamma P_0 \cos^2(\pi f_R \tau) + \Delta\beta_L$ is the phase matching term between the interacting waves, which is composed of the nonlinear phase shift $2\gamma P_0 \cos^2(\pi f_R \tau)$ that is time varying, and the linear phase shift $\Delta\beta_L = \sum_{k=1}^{2} \frac{\beta_{2k}}{(2k)!}\Delta\omega_S{}^{2k}$ that is constant in time. Equation (4) shows that the shape of the generated pulse on the idler side depends on the linear phase mismatch, and therefore on the signal position $\Delta\omega_S$ [1]. The phase term in Eq. (4) also shows two features: the generated pulses exhibit a chirp given by $\gamma P_0 \sin(2\pi f_R \tau)$, and they undergo a walk-off relative to the pump that is equal to $\beta_3 \Delta\omega_S^2/2$. The fact that the walk-off between the generated pulse and the pump depends only on the dispersion slope has already been experimentally demonstrated in parametric slow and fast light processes [15,16], as well as in modulation instability induced by a localized perturbation [17].

Assuming that the generated pulse width is short compared to the repetition period $1/f_R$, one can write to the second order $P_P(L,\tau) \approx P_0(1-(\pi f_R \tau)^2)$. We note that :

$$g = \sqrt{-\frac{\Delta\beta_L}{4}(4\gamma P_0 + \Delta\beta_L)\left(1 - \frac{4\gamma P_0}{4\gamma P_0 + \Delta\beta_L}(\pi f_R \tau)^2\right)} \approx g_0\left(1 - \frac{2\gamma P_0}{4\gamma P_0 + \Delta\beta_L}(\pi f_R t)^2\right)$$

where $g_0 = g(\tau = 0) = \sqrt{-\Delta\beta_L/4(4\gamma P_0 + \Delta\beta_L)}$. The approximation of g holds as long as the factor $\frac{2\gamma P_0}{4\gamma P_0 + \Delta\beta_L}$ is small. Since g is in the denominator of Eq. (4), one can safely use a Taylor expansion provided that $2\gamma P_0 < 4\gamma P_0 + \Delta\beta_L$, which is equivalent to $\kappa(\tau = 0) \geq 0$. Doing so, Eq. (4) becomes :

$$\begin{aligned} A_I(L,\tau) \quad &= jA_S^*(0)\frac{\gamma P_0}{g_0}\left[1 - \frac{2\gamma P_0 + \Delta\beta_L}{4\gamma P_0 + \Delta\beta_L}(\pi f_R t)^2\right]\sinh\left[g_0 L\left(1 - \frac{2\gamma P_0}{4\gamma P_0 + \Delta\beta_L}(\pi f_R t)^2\right)\right] \\ &\times e^{j\left[\gamma P_0 \cos^2(\pi f_R \tau)+\frac{\beta_3}{6}\Delta\omega_S{}^3\right]L} \end{aligned} \tag{5}$$

$\kappa(\tau = 0) \geq 0$ corresponds to the portion of the spectrum that is located between the pump location and the maximum gain location. For large $g_0 L$, one can write in the vicinity of $\kappa = 0$:

$$A_I = jA_S^*(0)\frac{\gamma P_0}{g_0}\frac{e^{\left\{g_0 L\left[1-\frac{2\gamma P_0}{4\gamma P_0 + \Delta\beta_L}(\pi f_R t)^2\right]\right\}+j\left\{\gamma P_0\left[1-(\pi f_R \tau)^2\right]+\frac{\beta_3}{6}\Delta\omega_S{}^3\right\}L}}{2} \tag{6}$$

We retrieve the formula of a Gaussian pulse found in [8]. In particular, for the exact phase matching case ($\kappa = 0$), the pulse FWHM is given by [1]:

$$T_{FWHM} = \frac{1}{\pi}\sqrt{\frac{2\ln 2}{\gamma P_0 L}} \times \frac{1}{f_R} \tag{7}$$

It is important to note that Eq. (6) is only valid for large $g_0 L$ and $\kappa(\tau = 0) \geq 0$, which represents a narrow portion of the gain bandwidth [1]. In all other cases, the FWHM must be calculated using Eq. (4). In particular, for $\kappa(\tau = 0) = -2\gamma P_0$, which corresponds to a signal located at the extremity of the parametric gain spectrum, we have $g \approx 2\pi j \gamma P_0 f_R \tau$ and :

$$A_I = jA_S^*(0)\gamma P_0 L \mathrm{sinc}(2\pi\gamma P_0 L f_R \tau) e^{j\left\{\gamma P_0 \cos^2(\pi f_R \tau)+\frac{\beta_3}{6}\Delta\omega_S{}^3\right\}L} \tag{8}$$

#174838 - $15.00 USD Received 23 Aug 2012; revised 15 Oct 2012; accepted 5 Nov 2012; published 19 Nov 2012

where the sinc function is defined as $\mathrm{sinc}(x) = \sin(x)/x$. In this case:

$$T_{FWHM} \approx \frac{0.443}{\gamma P_0 L} \times \frac{1}{f_R} \tag{9}$$

Equation (8) provides an alternative approach for all-optical generation of near-Sinc pulses that can have potential applications in Nyquist-WDM transmission and all-optical detection at the Nyquist limit. Note that for transmission applications, it would be necessary to remove the pump induced chirp. This can be done by using a phase modulator [18]. In the following section, we experimentally verify these theoretical findings. Note that these results are valid as long as: $2\pi/\Delta\omega_S << T_{FWHM} << 1/f_R$. For high repetition rate and/or highly compressed pulses, one must take into account the higher order signal and idler derivatives in order to calculate the generated pulse shape. A brief discussion of this case is given in the results and discussions section.

3. Experimental setup

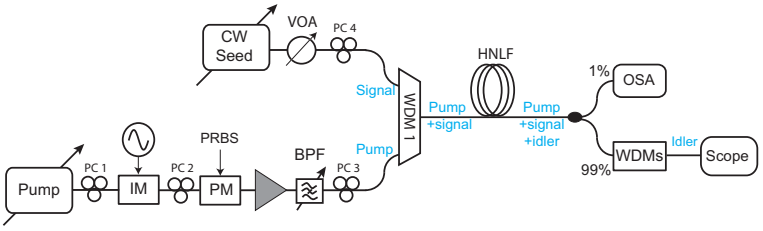

Fig. 1. Experimental setup. PC: polarization controller; IM: intensity modulator; PM: phase modulator; BPF: band pass filter; WDM: wavelength division multiplexer; HNLF: highly nonlinear fiber; OSA: optical spectrum analyzer.

The experimental setup is depicted in Fig. 1. The fiber optic parametric amplifier pump was constructed from a tunable high signal to noise ratio (SNR) continuous wave external cavity laser (CW ECL). The pump was amplitude modulated by a sinusoidal wave and subsquently phase modulated by a pseudo random bit sequence (PRBS) to suppress stimulated Brillouin scattering (SBS). Note that in order to suppress amplitude fluctuations that are induced by pump phase modulation on the generated pulse train, it is essential to delay the PRBS so that the pump phase jumps occur in between the generated pulses [1]. To this end, we used an RF phase shifter between the PRBS generator and the pump phase modulator (PM). The pump was amplified by an erbium doped fiber amplifier (EDFA) and filtered with a 2 nm band pass filter to suppress amplified spontaneous emission (ASE). A wavelength tunable CW ECL was used as a signal seed and its power was controlled by a variable optical attenuator (VOA). The pump and the signal were coupled through a wavelength division multiplexer (WDM) into a 500-m long segment of HNLF characterized by a $\gamma =$ 12 $\mathrm{W}^{-1}\mathrm{m}^{-1}$, a zero dispersion wavelength (ZDW) $\lambda_0 = 1551$ nm and a dispersion slope of 27.5×10^{-3} $\mathrm{ps.nm}^{-2}\mathrm{km}^{-1}$. The HNLF absorption was 0.75 dB/km leading to an effective length of $L_{eff} = 480$ m. At the output of the HNLF, a 1% tap was used to monitor the parametric process on the optical spectrum analyzer while the remainder of the light was connected to a cascade of WDMs in order to separate the generated idler from the signal and the high power pump. The idler was then observed on a high speed (500 GHz) optical sampling oscilloscope and an optical spectrum analyzer with down to 0.02 nm resolution.

The wavelength of the signal seed was swept between the Gaussian position ($\Delta\beta_L = -2\gamma P_0$) and beyond the Sinc shape position ($\Delta\beta_L = -4\gamma P_0$). The effects of signal seed power on the

#174838 - $15.00 USD Received 23 Aug 2012; revised 15 Oct 2012; accepted 5 Nov 2012; published 19 Nov 2012

pulse generation as well as pump position were evaluated. The obtained experimental results were compared to theoretical calculations and simulations and are presented in the following section.

4. Results and discussions

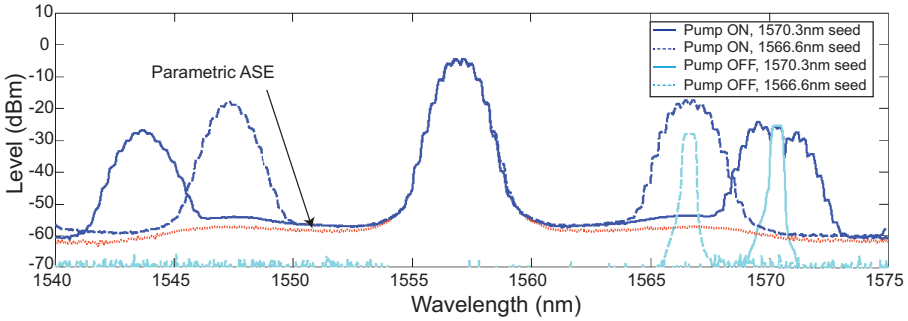

Fig. 2. Optical spectra at the output of the HNLF for pump OFF and ON and for no signal seed (parametric ASE, dotted line), signal seed positions of 1566.6nm and 1570.3nm.

The pump, modulated with a 40 GHz sinusoidal wave, was first positioned at 1557 nm, in the anomalous dispersion regime, with an average power inside the HNLF of 410 mW. Taking into account the dispersion of the HNLF, the pump wavelength and power, the Gaussian shape position was calculated for a signal seed wavelength of 1566.6 nm and the Sinc shape position at the edge of the gain spectrum for a signal seed wavelength of 1570.3 nm. The optical spectra at the output of the HNLF (1% tap) for the input seed at 1566.6 nm and 1570.3 nm are shown in Fig. 2. A gain close to 14 dB, taking into account pulsing of the signal, was experienced at the perfect phase matching point, while 3 dB gain was measured at the edge of the gain spectrum. The waveform of the generated idlers observed on the 500 GHz optical sampling scope for these two different signal seeds as well as for a 1570.5 nm seed, are shown in Fig. 3(a), (d) and (g). The generated idler not only shows a significant compression compared to the input sinusoidal wave but also a different shape depending on the linear phase mismatch, as expected from the theory. The optical spectrum of the idler was retrieved with a 0.02 nm resolution as shown in Fig. 3(b), (e) and (h), for the three seed positions respectively. The shape of the spectra evolves along with the pulses temporal shape. Close to the Sinc shape position, the spectrum bandwidth is slightly larger due to the reduced pulse width. As a consequence of the chirp induced by the parametric pump, the power spectral densities are redistributed to the higher harmonics. By dechirping the generated pulses, it is possible to obtain a more squared spectrum [18]. Beyond the Sinc point, the optical spectrum became slightly distorted. Numerical simulations of the nonlinear Schrödinger equation taking into account fiber loss and pump noise were also performed. The experimental results, theoretical fit as well as simulation results obtained from the VPIphotonics^{TM} platform are shown in Fig. 3(c), (f) and (i). Excellent agreements were obtained between the experiment and the simulations, not only in terms of generated pulse width and shape but also noise. The theoretical fits, using the effective length, confirmed the expected linear mismatch: a $\Delta\beta_L = -2.2032\gamma P_0$ was retrieved from the 1566.6 nm seed results, thus close to the expected Gaussian point. A $\Delta\beta_L = -3.9753\gamma P_0$ perfectly matches the Sinc position for the 1570.3 nm, while a slightly detuned signal at 1570.5 nm goes beyond the $\Delta\beta_L = -4\gamma P_0$ point for a generated idler pulse distorted from the Sinc shape.

The wavelength of the signal seed was then swept between 1565 nm and 1572.8 nm. The

#174838 - $15.00 USD Received 23 Aug 2012; revised 15 Oct 2012; accepted 5 Nov 2012; published 19 Nov 2012

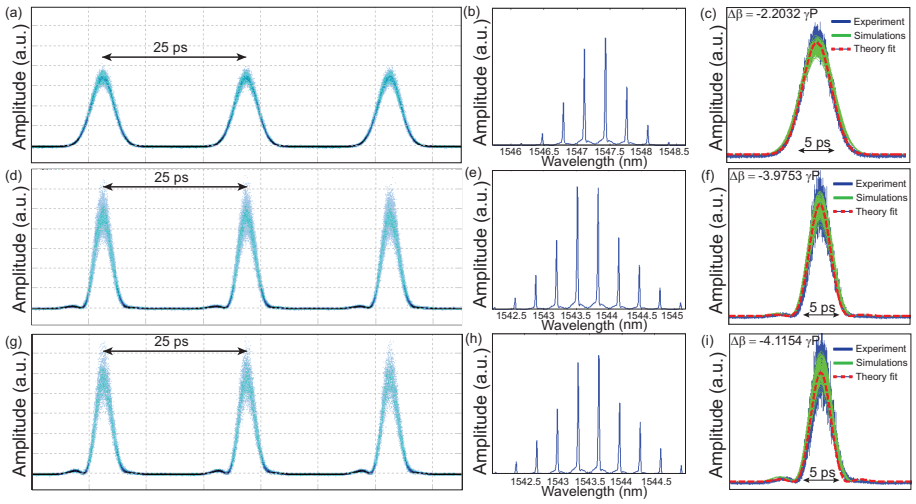

Fig. 3. Results for 1557 nm pump. (a) Idler waveform and (b) spectrum for 1566.6nm signal; (c) Experiment, simulations and theoretical fit for 1566.6 nm signal corresponding to $\Delta\beta_L = -2.2032\gamma P_0$; (d)Idler waveform and (e) spectrum for 1570.3 nm signal; (f) Experiment, simulations and theoretical fit for 1570.3nm signal corresponding to $\Delta\beta_L = -3.9753\gamma P_0$;(g)Idler waveform and (h) spectrum for 1570.5nm signal; (i) Experiment, simulations and theoretical fit for 1570.5 nm signal corresponding to $\Delta\beta_L = -4.1154\gamma P_0$.

pump was moved to 1556 nm in order to optimize the utilization of the WDMs used for pump stripping/idler selection and thus cover the widest range of generated idlers. In this configuration, idler pulses were observed between 1539.5 nm and 1547.1 nm. The sweep was realized for three different seed laser powers: 0 dBm, 3 dBm and 6 dBm. An EDFA operating in a constant power mode was placed before the oscilloscope in order to maintain the same average power at the detector throughout the sweep. The results are shown in Fig. 4. For a low input seed power (Fig. 4(a)), the generated idler pulse shape evolved from a Gaussian towards a Sinc shape. When the seed exited the parametric gain bandwith, strong distortions of the pulse were observed. The FWHM of the generated pulse became shorter as the seed signal moved from the maximum gain to the edge of the gain spectrum leading to a higher peak power. For a high seed power (Fig. 4(c)), the pump was depleted by the signal near the maximum gain region leading to a widened and distorted pulse shape. As the seed signal moved away from perfect phase matching, the decrease in parametric gain resulted in less pump depletion and pulse shapes similar to the low power case were observed. The evolution of the FWHM as a function of seed wavelength for 0, 3 and 6 dBm of power is plotted in Fig. 4(b). For low seed power, a constant width was measured near the perfect phase matching point (Gaussian shape). The width then decreased as the seed approached the edges of the gain bandwidth and reached the Sinc shape point. As the seed power increased, wider pulse widths were measured near the Gaussian point due to pump depletion. When the seed approached the edge of the parametric gain, all curves converged, as expected. For a 0 dBm seed, a comparison between the experimentally measured FWHM, the FWHM from numerical simulations and the theoretical values without pump depletion from Eq. (4) are shown in Fig. 4(d). A very good agreement was found.

The seed power also has an impact on the quality of the generated pulse as shown in Fig. 5. The pump wavelength was set at 1556 nm with a peak pump power of 650 mW. The signal wavlengths were set at 1568.6 nm, 1570 nm and 1572 nm, which approximately corresponded to $\Delta\beta_L = -2\gamma P_0$, $\Delta\beta_L = -3\gamma P_0$ and $\Delta\beta_L = -4\gamma P_0$, respectively. For each position, the seed

#174838 - $15.00 USD Received 23 Aug 2012; revised 15 Oct 2012; accepted 5 Nov 2012; published 19 Nov 2012

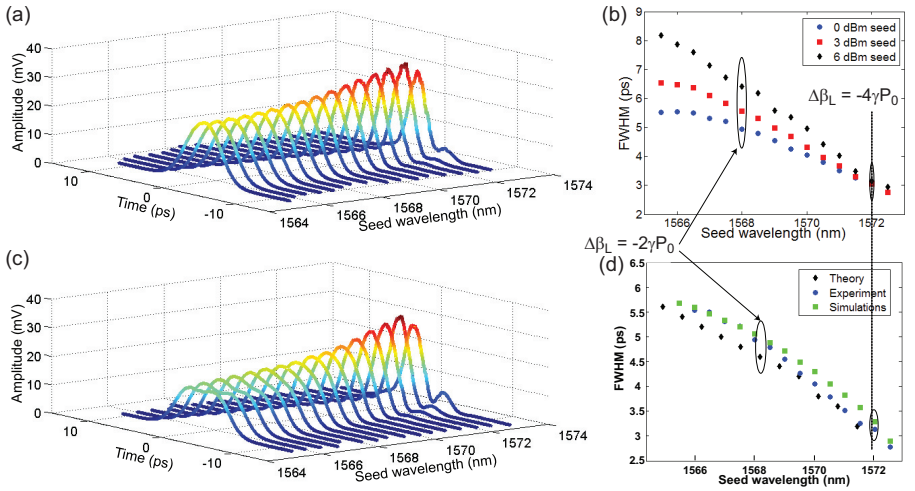

Fig. 4. Idler pulse shape evolution as a function of input seed wavelength for (a) 0 dBm of seed power and (c) 6 dBm of seed power. (b) Experimental full width half max (FWHM) of generated idler pulse as a function of seed wavelength for 0, 3 and 6 dBm of seed power and (d) Comparison of the measured, simulated and theoretical FWHM of generated idler for 0 dBm of seed power.

power was swept from 0 dBm to 6 dBm. At 0 dBm, we observed that the generated pulses exhibit more noise as they were located further from the pump. Indeed, as $\Delta\omega_S$ increases, $\Delta\beta_L$ decreases and as a result, the parametric gain becomes more sensitive to perturbations of the pump power [1]. Note that similar observations have been made in studies of noise and signal deterioration in CW-pumped fiber OPAs [19, 20]. When the seed power increased, the pulse peak was clipped because of saturation at the maximum peak gain location ($\lambda_S = 1568.4$ nm, $\Delta\beta_L = -2\gamma P_0$). At higher signal detuning, saturation was avoided while simultaneously the generated pulses exhibited less noise as more idler power was available at the detector. For every signal position, there is an optimum seed power that lowers the generated pulse noise and avoids pump depletion. The signal to noise ratio (SNR) for each pulses of Fig. 5 was calculated from the collected data. The mean (P_{one}) and standard deviation (σ_{one}) within a 1 ps window at the peak of the pulse was retrieved and then used to obtain $SNR = 20 \times \log 10(P_{one}/\sigma_{one})$. The results are shown in table 1.

Table 1. SNR (dB) of generated pulses

Signal seed power (dBm)	$\Delta\beta_L = -2\gamma P_0$ (Gaussian)	$\Delta\beta_L = -3\gamma P_0$	$\Delta\beta_L = -4\gamma P_0$ (Sinc)
0	27.58	22.43	15.9
3	31.15	25.78	19.2
6	31.38	30.13	20.9

Figures 5(g), (h) & (i) also show that the generated pulses exhibit a small asymmetry. This asymmetry is due to walk-off, as shown in Fig 6(a), (b) & (c). Indeed, for a lower repetition rate of 2.75 GHz, we observe no asymmetry. As the repetition rate increases, the signal, pump and idler pulses become shorter. Because of walk-off, they lose their overlapping along propagation in the HNLF, which leads to some asymmetry on the generated pulse. Walk-off therefore

#174838 - $15.00 USD Received 23 Aug 2012; revised 15 Oct 2012; accepted 5 Nov 2012; published 19 Nov 2012

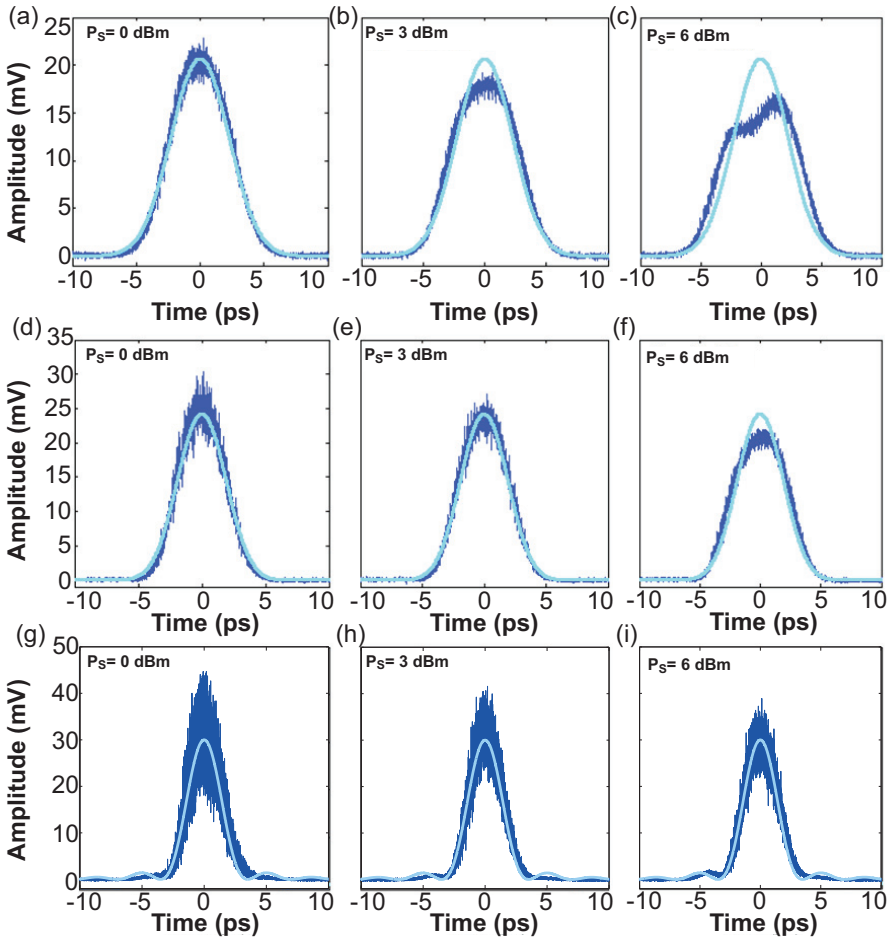

Fig. 5. Idler pulse shapes for (a), (b) & (c) $\Delta\beta_L = -2\gamma P_0$, (d), (e) & (f) $\Delta\beta_L = -3\gamma P_0$ and (g), (h) & (i) $\Delta\beta_L = -4\gamma P_0$ and different signal input powers.

constitutes a strong limitation for generating symmetric pulses at high repetition frequency. In order to investigate this, it is necessary to take into account the first order derivative of the SVEs in Eq. (2). We then align the fields phases with the pump phase rotation: $B_S = A_S e^{j\gamma P_0 \cos^2(\pi f_R \tau) z}$. We also consider that $\left|\frac{\partial B_S}{\partial \tau}\right|^2 << |B_S|\gamma P_0 z \pi f_R$. Making the following change of variable:

$$B_k = C_k e^{\alpha_k j\left[\frac{\beta 3}{6}\Delta\omega^3 z + \gamma P_0 \pi f_R \sin(2\pi f_R \tau)\left(\frac{\beta_2}{2}\Delta\omega + \frac{\beta_4}{12}\Delta\omega^3\right)z^2\right]} \quad k = \{S, I\}$$

with $\alpha_I = +1$ and $\alpha_S = -1$, one can then straightforwardly derive the following equation:

$$\frac{\partial^2 C_{S,I}}{\partial z^2} = \left[\left(\gamma P_0 \cos^2(\pi f_R \tau)\right)^2 - \left(\frac{\kappa + WOz}{2}\right)^2 + j\frac{WO}{2}z\right] C_{S,I} \tag{10}$$

where $WO = \beta_3 \gamma P_0 \pi f_R \sin(2\pi f_R \tau)\Delta\omega_S{}^2$. The solutions of Eq. (10) can be described with complicated hypergeometric functions, which do not provide a valuable physical insight [14]. However, Eq.(10) shows that the phase matching κ is incremented by WOz, which depends on the

#174838 - $15.00 USD Received 23 Aug 2012; revised 15 Oct 2012; accepted 5 Nov 2012; published 19 Nov 2012

fiber dispersion slope and the pump derivative. It shows that the phase matching term is increased for shorter times and decreased for longer times. Hence, in the case of near-Sinc pulses, there will be more gain at shorter times and less gain at longer times compared to the ideal case. Furthermore, we notice that a higher signal to pump frequency detuning $\Delta\omega_S$ will increase that asymmetry. This is particularly detrimental for the generation of near-Sinc pulses since they are located at the edge of the gain spectrum. We have verified this behavior in Fig. 6(d), which shows the simulation of the generated Sinc pulses for a pump located at 1556 nm and 1552 nm. We observe that when the pump is located at 1552 nm, the Sinc shaped pulse is generated further from the pump and as a result, there is more asymmetry. Replacing κ with $\kappa + WO \times L$ in Eq. (4) also provides a good agreement with the simulations (Figs. 6(e) & (f)), hence reinforcing the physical insight of Eq. (10).

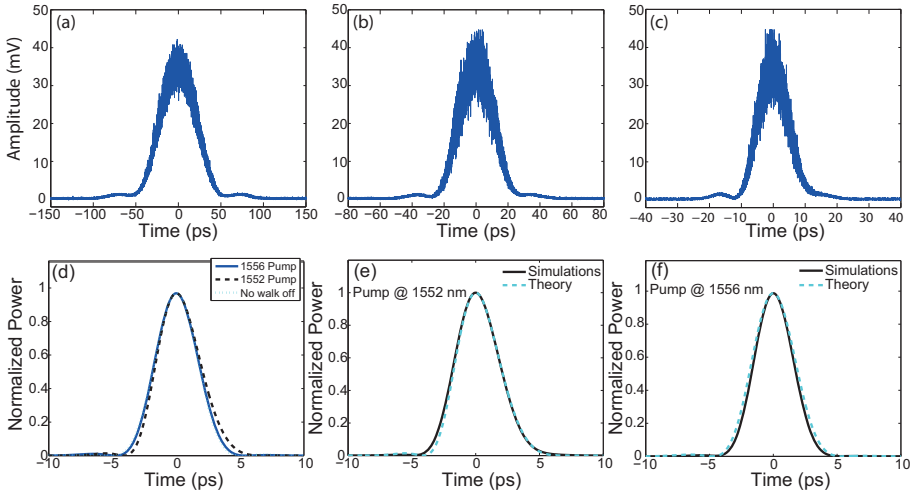

Fig. 6. Idler waveform at the near-Sinc shape position for frequency repetition (a) 2.75 GHz, (b) 5.5 GHz and (c) 11 GHz. (d) Comparison of the idler pulse shapes for $\Delta\beta_L = -4\gamma P_0$ with pump wavelength at 1552 nm (dashed line), 1556 nm (solid line) and theoretical fit from Eq. (8) at 40 GHz repetition rate. Simulations (solid line) and theoretical fit using $\kappa + WO \times L$ in Eq. (4) for pump wavelength at (e) 1552 nm & (g) 1556 nm at 40 GHz repetition rate.

5. Conclusion

We verified experimentally the theory introduced in [1]. We proved mathematically that the generated pulses can be assumed to be Gaussian only for high $g_0 L$ and $\Delta\beta_L \geq -2\gamma P_0$. The results obtained experimentally showed excellent agreement with the theory. In particular, we showed that it is possible to generate all-optically near-Sinc pulses at repetition rate as high as 40 GHz. At that repetition rate, the pulse FWHM was measured at 3.5 ps, which represents a compression by a factor of 7. By numerical simulations, we also investigated the impact of pump saturation and seed power on the quality of the generated pulses. We found good agreement with the experimental results and showed that for every linear phase mismatch, the seed power can be optimized in order to lower the generated pulse noise. Furthermore, we investigated the impact of walk-off and revealed that the generated pulse exhibits an asymmetry that is due to the dispersion slope and the pump time derivative. The ability to generate pulses of different shapes (Gaussian, Sinc ...) opens up the path for a variety of applications in ultrafast all-optical signal processing. In particular, when the signal is located at the edge of the FOPA

#174838 - $15.00 USD Received 23 Aug 2012; revised 15 Oct 2012; accepted 5 Nov 2012; published 19 Nov 2012

spectrum, it is possible to generate near-Sinc pulses. Using these pulses for transmission requires removing the pump induced chirp. But the possibility to generate a window in the time domain with a near-Sinc shape response allows for the development of all-optical Nyquist limited receivers and samplers. However, this regime is also the most sensitive to tiny fluctuations of the pomp power and to walk-off. In order to fully exploit these near-Sinc pulses, the development of viable low-noise sinusoidal pumps or new architectures employing two dissimilar frequencies pumps is necessary.

Acknowledgment

The authors thank Thibaut Sylvestre of Femto-ST Institute for the loan of the HNLF fiber. Mehdi Alem Karladani, Gil Fanjoux and Arnaud Mussot are acknowledged for fruitful discussions.

#174838 - $15.00 USD Received 23 Aug 2012; revised 15 Oct 2012; accepted 5 Nov 2012; published 19 Nov 2012